Journal of Membrane Science 684 (2023) 121880

Contents lists available at ScienceDirect

Journal of Membrane Science

journal homepage: www.elsevier.com/locate/memsci

Rapid synthesis of ultrathin covalent organic polymer membranes with subnanometer pores for efficient organic solvent nanofiltration

Jianghai Long, Xiansong Shi **, Tong Ju, Xingyuan Wang, Zhe Zhang, Yong Wang *

State Key Laboratory of Materials-Oriented Chemical Engineering, College of Chemical Engineering, Nanjing Tech University, Nanjing, 211816, Jiangsu, PR China

ARTICLE INFO

Keywords:
Organic solvent nanofiltration
Covalent organic polymers
Interfacial synthesis
Separation membrane
Transition-metal nitrates

ABSTRACT

Covalent organic polymers (COPs) with abundant micropores are deemed as promising materials for building molecular separation membranes. In spite of this potential, fabricating COP separation membranes through an efficient and scalable method remains a significant challenge. Herein, we report a simple and efficient strategy for the synthesis of COP membranes with three-dimensionally interconnected micropores. Utilizing transition-metal nitrates as a catalyst, we achieve fast polymerization of amorphous COPs with relatively uniform micropores (0.7 nm in diameter). The rational design of organic-aqueous interface allows for the direct fabrication of robust COP membranes with an ultrathin thickness of ~20 nm on porous polyacrylonitrile substrates. The resulting hydrophobic but pore-uniform frameworks in these membranes permit fast permeation of organic liquids with a notable molecular weight cutoff of 388 g mol^{-1} in ethanol. To demonstrate scalability, we show that our strategy can produce large-size COP membranes with a prominent area of 200 cm^2, which exhibit performances similar to that of small membrane coupons. The present study offers a potentially scalable method for producing highly microporous COP membranes toward efficient molecular separation in organic liquids.

1. Introduction

At present, organic liquids are indispensable auxiliaries in a range of chemical processes, including petrochemical industries, pharmaceutical manufacturing, and organic synthesis [1–4]. However, their large quantities involved in the production processes pose a huge challenge for the concentration of products as well as the recovery of solvents [5,6]. Conventional separation technologies, such as evaporation, distillation, and liquid-liquid extraction, have been widely used to tackle the above issues, but the limitations including high energy consumption and relatively tedious procedures hinder their sustainable development [7,8]. Organic solvent nanofiltration (OSN) enabled by membrane technologies has emerged as a promising and environmentally friendly alternative [9,10]. OSN is characterized by its low energy consumption, high processing efficiency, and low carbon footprint. To be specific, compared to traditional energy-intensive technologies, OSN could save up to 90% energy [11,12]. Typically, OSN membranes should be provided with molecular sieving channels below 2 nm to separate fine solutes with molecular weights of 200–1000 g mol^{-1} while maintaining desirable permeance and stability toward organic solvents [13,14]. It is worth noting that the current demand for OSN membranes is rapidly growing because of the real-world needs to selectively separate small but size-similar products at little expense of energy [15,16]. Thus, in response to the revolution of existing separation processes, developing advanced OSN membranes with excellent performances and practicality has become imperative.

Traditional polymer materials, such as polyimide (PI), polybenzimidazole (PBI), polyamide (PA), polyaniline (PANi), and polyether ether ketone (PEEK), have been utilized for the exploration of OSN membranes [17–20]. However, the chemical instability including structural swelling and physical aging in continuous operations is regarded as a major limitation that debases membrane performance and durability [21]. To overcome structural deterioration, a range of strategies including chemical cross-linking and thermal treatment have been developed to improve material stability and thus membrane durability [22–24]. Nevertheless, these treatments in turn lead to significantly reduced solvent permeance due to the limited mass transport efficiency in hyper-cross-linked networks [25]. Alternatively, researchers are exploring highly crystalline materials with ordered channels and permanent porosities to build novel OSN membranes [26,27].

* Corresponding author.
** Corresponding author.
E-mail addresses: xsshi@njtech.edu.cn (X. Shi), yongwang@njtech.edu.cn (Y. Wang).

https://doi.org/10.1016/j.memsci.2023.121880
Received 26 April 2023; Received in revised form 18 June 2023; Accepted 22 June 2023
Available online 25 June 2023

Metal-organic frameworks (MOFs) and covalent organic frameworks (COFs) are deemed as the prototypical crystalline materials and have been constructed into membranes for high-selectivity separation of ultrafine species including gases, ions, and organic molecules [28–32]. Despite their prominent separation performances, the building of crystalline MOF and COF membranes usually requires considerable synthetic durations (12–72 h) and harsh conditions [33,34]. The complicated synthesis of crystalline membranes accordingly limits their potential for large-scale OSN membrane production and practical applications. Therefore, a balance between material benefits and membrane synthesis is pending to be reasonably optimized, which may promote the development of high-performance OSN membranes featuring easy synthesis and scalability.

Covalent organic polymers (COPs) are a type of noncrystalline porous materials constructed by linking organic building blocks through covalent bonds. In sharp contrast to crystalline COFs with long-range ordered pores, amorphous or semi-crystalline COPs typically exhibit disordered pores with a relatively narrowed size distribution [35,36]. Consistent with COFs, COPs also exhibit desirable solvent resistance due to their extended covalent bonds [37,38]. Fortunately, different from the synthesis of high-crystallinity COFs, which mostly requires time-consuming and harsh processes for self-correction, COPs are usually synthesized through straightforward procedures and mild conditions, with a short reaction time [39,40]. More importantly, robust covalent bonds in COPs can prevent the framework structure from twisting, thus allowing the generation of pores with a comparatively narrow size distribution [41]. These distinctive features of COPs potentially allow fast permeation of solvents with no significant loss of selectivity. For example, Szekely and coworkers reported that a fluorine-containing COP membrane can yield a high rejection of up to 95% to Congo red with an efficient toluene flux of 11 L m^{-2} h^{-1} [42]. Thus, the exploration of COP membranes not only offers an avenue for easily synthesizing advanced OSN membranes under mild conditions, but also provides an opportunity to gain insights into the correlation between separation performance and material crystallinity.

In this work, we demonstrate a rapid way to fabricate a three-dimensional COP and its composite membranes under ambient temperature. By applying transition-metal nitrates ($Cu(NO_3)_2$) as the catalyst, the condensation of monomer pairs can be performed immediately. The obtained COPs are featured with an amorphous structure, while gas sorption analysis reveals their highly porous configuration with a sharp pore size distribution. With the assistance of $Cu(NO_3)_2$ and interfacial strategy, we further realize the synthesis of COP membranes within 10 min. Applying this interfacial protocol on porous substrates, composite membranes with an ultrathin layer of COPs as the selective layer are obtained. The membrane thicknesses and thus separation performances can be easily controlled by altering the synthetic conditions including catalyst concentration and reaction time. The optimized composite membrane exhibits a high rejection rate of 99% to acid fuchsin under a decent ethanol permeance of 14.5 L m^{-2} h^{-1} bar^{-1}, thanks to the spatially interpenetrated pores with a uniform size. Particularly, large-size COP composite membranes (~200 cm^2) with a comparable performance also can be produced by the same preparation procedures. The proposed method is expected to efficiently fabricate diverse covalent organic polymer membranes for practical applications.

2. Experimental section

2.1. Materials

Tetrakis(4-formylphenyl)-methane (TFPM, 98%), 2,4,6-triformylphloroglucinol (98%), 1,3,5-benzenetricarboxaldehyde (99%), and tetrakis(4-aminophenyl)methane (99%) were purchased from Jilin Chinese Academy of Sciences-Yanshen Technology. Hydrazine hydrate (HZ, 85%) was supplied by Sinopharm Chemical Reagent. *o*-Xylene (99%) was purchased from Energy Chemical. *p*-Phenylenediamine (99%), *N*, *N*-dimethylformamide (DMF, 99.5%), and 1,4-dioxane (99%) were supplied by Aladdin. Copper nitrate hydrate ($Cu(NO_3)_2$, 99.99%) was purchased from Macklin. Polyacrylonitrile (PAN, 85000 g mol^{-1}) powders and non-woven fabrics were supplied by local suppliers. Polyethylene glycol 400 (PEG400, 99.9%) was obtained from Shanghai Lingfeng Chemical Reagent. Hexane (98%), acetone (99.5%), acetonitrile (99%), tetrahydrofuran (THF, 99%), methanol (MeOH, 99.5%), ethanol (EtOH, 99.7%), propanol (99.5%) and butanol (99%) were used to assess solvent permeances. Mordant orange 1 (MO-1), methyl orange (MO), eriochrome black T (EB-T), acid fuchsin (AF), Congo red (CR), and Evans blue (EB) were purchased from Institute of Chemical Reagent. Anodic aluminum oxide (AAO) substrates (ø = 2.5 cm, nominal pore diameter: 0.1 μm) were obtained from Whatman. Deionized water (DI water, conductivity: ~2–10 μS cm^{-1}) was used throughout the study. All chemicals and reagents were used without further purification.

2.2. Preparation of porous PAN substrates

Porous PAN substrates were prepared by the process of non-solvent-induced phase separation. Specifically, PAN powders (11 g) were vacuum dried at 80 °C for at least 12 h. Then, the powders and PEG400 (porogen, 4 g) were dissolved in DMF (85 g) to form a polymer dope. The dope was mechanically stirred at 60 °C for 12 h for complete dissolution and then degassed at room temperature for at least 24 h to obtain a homogeneous casting solution. The solution was cast with a 200-μm thick blade on the non-woven fabric, which was immediately immersed in DI water for phase inversion. After that, the obtained PAN porous substrates were stored in DI water before further characterization and use. The obtained PAN substrate exhibits a pure water permeance of ~900 ± 50 L m^{-2} h^{-1} bar^{-1}.

2.3. Synthesis of COP powders

TFPM (86.4 mg, 0.2 mmol) and HZ (30 μL) were dispersed in 5.2 mL 1,4-dioxane followed by sonication for 2 min. Next, 0.8 mL $Cu(NO_3)_2$ aqueous solution (0.05 mol L^{-1}) was added to the mixture. The mixture was then left undisturbed at room temperature for 1, 6, 12, and 24 h, respectively. The obtained products were washed with 1,4-dioxane and THF by filtration to eliminate residual unreacted monomers, and then vacuum dried at 80 °C overnight.

2.4. Fabrication of free-standing COP membranes

As shown in Fig. S1, silicon wafers were placed on the bottom of a glass vessel (ø = 7 cm) before adding $Cu(NO_3)_2$ aqueous solution (30 mL, 0.05 mol L^{-1}). TFPM (8 mg) and HZ (6 μL) were separately dissolved in *o*-xylene (20 mL). Then, a 30-mL mixture containing an equal volume of the TFPM and HZ solutions was gently added onto the aqueous phase. The glass vessel was kept under room temperature for designated durations. The membranes formed at the organic-aqueous interface were transferred onto silicon wafers and AAO substrates for further characterization.

2.5. Fabrication of COP composite membranes

COP composite membranes were interfacially synthesized on porous PAN substrates. The PAN substrates were cut into small membrane coupons with a diameter of ~4.5 cm and immersed in $Cu(NO_3)_2$ aqueous solutions overnight. Then, the PAN coupon was horizontally placed in the middle of a homemade synthesis device and fixed by clamps. After pouring off the aqueous solution, kimwipes were used to remove residual water droplets on the PAN surface. Next, a 15-mL mixture of the monomer solutions was immediately added on the surface of PAN substrate. The interfacial polymerization occurred for designated durations. The resulting membranes were thoroughly rinsed with EtOH and stored in EtOH for further use. To directly characterize the formed COP layers,

the composite membranes were immersed in DMF to degrade PAN substrates and the obtained COP layers were transferred onto silicon wafers for further characterizations. The large-size COP composite membranes (20 × 10 cm^2) were fabricated under the same synthesis parameters and conditions as the aforesaid procedure with a larger apparatus.

2.6. Filtration tests

The filtration tests were carried out by a stainless dead-end filtration device with an effective area of ~10.2 cm^2 under 1 bar to assess OSN performances of membranes. The membranes needed to be pre-pressed at 1 bar for at least 30 min to reach steady permeation before the tests. In filtration tests, three membranes prepared at the same condition were evaluated to present the corresponding average value and error bar. The solvent permeation flux (J, L m^{-2} h^{-1}) and permeance (P, L m^{-2} h^{-1} bar^{-1}) of membranes were calculated by the following equations:

$$J = V/(A\ \Delta t)$$

$$P = V/(A\ \Delta t\ \Delta p) = J/\Delta p$$

where V (L) represents the volume of the solvent that permeates across the effective membrane area A (m^2) in a predetermined permeation duration Δt (h) under the cross-membrane pressure Δp (bar).

Dyes dispersed in EtOH and MeOH with a concentration of 10 ppm were used as the feed to evaluate the molecular sieving performances of membranes. The filtration tests were conducted under continuous stirring at 300 rpm to reduce concentration polarization. The dye concentrations were analyzed by an ultraviolet and visible (UV–vis) spectrophotometry absorption spectrometer (NanoDrop 2000C, Thermo Fisher). The dye rejection rate (R, %) was calculated by the following equation:

$$R = (1\text{-}C_p/C_f) \times 100\%$$

where C_p and C_f are the dye concentration of the permeate and feed, respectively.

2.7. Characterizations

Fourier transform infrared (FTIR, Nicolet 8700) spectroscopy was utilized to study the chemical compositions of the monomers, COP powders, and membranes with the wavenumber ranging from 500 to 4000 cm^{-1}. Potassium bromide pressed pellet method and attenuated total reflection mode were used for particulate and membrane tests, respectively. The membranes and powders were imaged by field-emission scanning electron microscopy (SEM, Hitachi S-4800) at an accelerating voltage of 5 kV after Au coating. For cross-sectional imaging, the membrane samples were wetted by EtOH and then cryogenically fractured in liquid nitrogen. Surface morphologies and membrane thicknesses were examined by atomic force microscopy (AFM, XE-100, Park Systems) at a noncontact mode. The AFM images with a boundary of membranes and silicon wafers were collected to determine the thickness by creating a height profile. The thickness of the free-standing membranes was also determined using a spectroscopic ellipsometer (Complete EASE M−2000U, J. A. Woollam). Transmission electron microscopy (TEM) was operated using a FEI Talos F200X G2 electron microscope at a voltage of 200 kV. The composite membrane was implanted into epoxy resin followed by microtoming using a diamond knife to obtain a cross-sectional slice. The slice was transferred onto a copper grid for TEM characterizations. Powder X-ray diffraction (PXRD) patterns of COP powders were measured at room temperature with a 2 theta range of 2–40° and a step size of 0.02° s^{-1} (Rigaku SmartLab). Nitrogen adsorption-desorption measurements of COP powders were conducted by a surface area and porosity analyzer (BELSORP MAX) at 77 K. Brunner−Emmett−Teller (BET) surface areas and pore width distributions were obtained by the sorption curves based on the nonlocal density functional theory (NLDFT). The solvent wettability of composite membranes was obtained by a contact angle goniometer (DropMeter A100, Maist). Zeta potentials of the composite membranes and PAN substrates were measured by an electrokinetic analyzer (Surpass 3 Anton Paar, Austria). The Zeta potential of dye solutions was tested by Malvern Zetasizer Nano ZS90 system.

3. Results and discussion

In this study, we synthesized a three-dimensionally interconnected microporous COP through the condensation of TFPM and HZ using Cu$(NO_3)_2$ as the catalyst (Fig. 1a). Without Cu$(NO_3)_2$, the COP powders could only be produced in small amounts (Fig. S2), indicating the highly efficient catalysis of Cu$(NO_3)_2$ at room temperature [43,44]. SEM characterization reveals that the lateral size of the synthesized COPs keeps about 2 μm without showing significant changes when the synthetic duration prolongs from 1 to 24 h (Fig. S3). The FTIR measurement of COPs synthesized for 24 h shows a new characteristic peak at ~1621 cm^{-1} (C═N) (Fig. 1b), indicating the formation of imine-based linkages [45]. Moreover, we can observe an intense stretching vibration arising from C═O at 1699 cm^{-1} in the synthesized COPs. The peak is attributed to the unreacted aldehyde groups of TFPM, which indicates imperfect polymerization between TFPM and HZ. Accordingly, the resultant COPs exhibit an amorphous structure as confirmed by the PXRD results (Fig. 1c), differing from the previously reported crystalline COFs [46,47]. The utilization of Cu$(NO_3)_2$ as the catalyst and the mild synthesis conditions collectively lead to this amorphous structure. N_2 sorption tests were subsequently adopted to investigate the porous structure of COPs. Fig. 1d shows the N_2 adsorption-desorption isotherms at 77 K, and the notable gas uptake at the low relative pressures discloses that COPs feature a highly microporous structure in spite of their amorphous nature. The BET surface area of COPs is determined to be ~278 m^2 g^{-1}, and the NLDFT fitting further reveals a sharp pore size distribution centered at ~0.7 nm (Fig. 1e). Thus, Cu$(NO_3)_2$ effectually promotes the polymerization of monomer pairs, resulting in amorphous but microporous COPs with relatively uniform subnanometer channels available for sharp separations [48].

The efficient polymerization enabled by Cu$(NO_3)_2$ motivates us to study the possibility of preparing the relevant membranes for separations. To this end, we elaborately designed an organic-aqueous interface for the direct synthesis of COP membranes. Specifically, monomer pairs dispersed in *o*-xylene and Cu$(NO_3)_2$ dissolved in DI water were used as the organic and aqueous phases, respectively (Fig. S4a). As expected, we can observe the generation of a thin membrane at the designed interface within 10 min (Fig. 2a). Considering the Lewis acid catalytic role of Cu$(NO_3)_2$, its diffusion from the aqueous phase to the organic phase rationalizes the growth of membranes at the interface [49]. As a contrast, the absence of Cu$(NO_3)_2$ in aqueous solution and the conventional synthesis by separately dissolving monomers in organic and aqueous solutions both produce no membranes (Figs. S4b and c). The SEM observation reveals that the resulting membrane supported by a porous alumina substrate features a smooth surface (Fig. 2b). Moreover, the integrity of these interfacially synthesized membranes is largely improved with the prolonging of synthesis durations, eventually yielding a defect-free membrane at 30 min (Fig. S5). The cross-sectional view in Fig. 2c obviously recognizes a continuous membrane with a low thickness of ~40 nm. Fig. 2d shows the AFM image of the membrane on a silicon wafer, which determines an identical thickness to that of the SEM result (Fig. 2e). In addition, this interfacial strategy allows a control of membrane thicknesses by altering the synthetic durations. As shown in Fig. 2f, the results determined by spectroscopic ellipsometry tests present the thickness variation of the membranes produced with various reaction durations. Obviously, the membrane thickness can be precisely regulated in the range of ~10–55 nm, indicative of the control over membrane growth. Thus, the utilization of this organic-aqueous

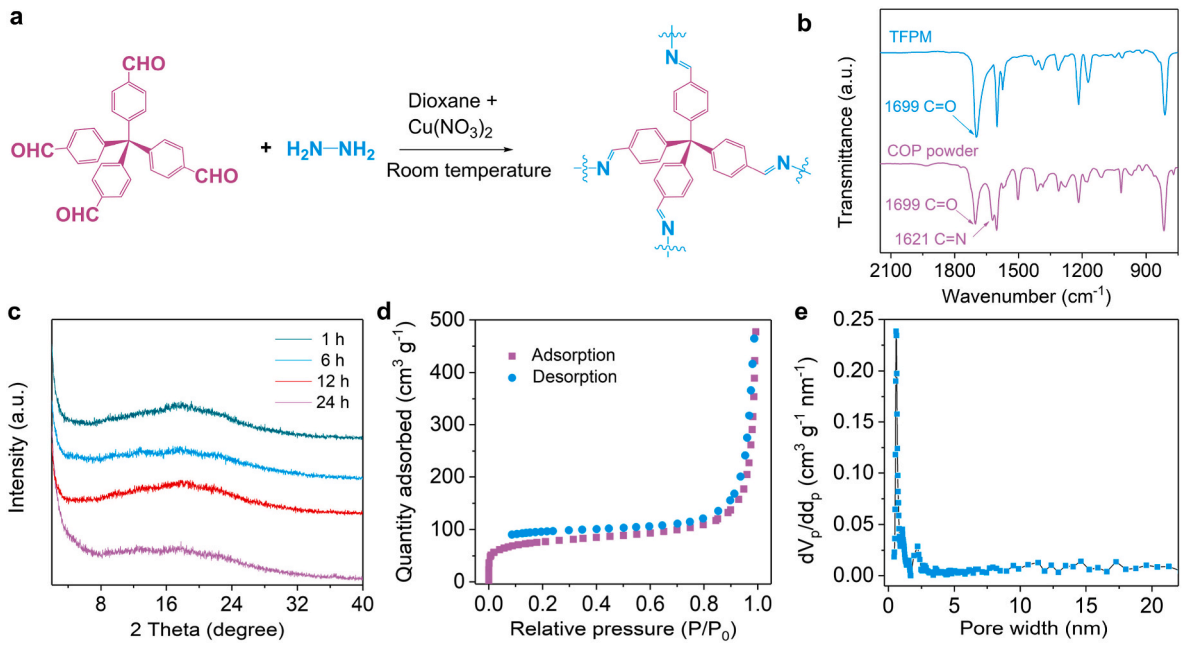

Fig. 1. Synthesis and characterization of COPs. (a) Schematic diagram for the synthesis of COPs. (b) FTIR spectra of TFPM and COPs synthesized for 24 h. (c) PXRD patterns of the COP powders produced with various synthesis durations. (d, e) N_2 adsorption-desorption isotherms of the COP powders synthesized for 24 h and the corresponding pore width distribution.

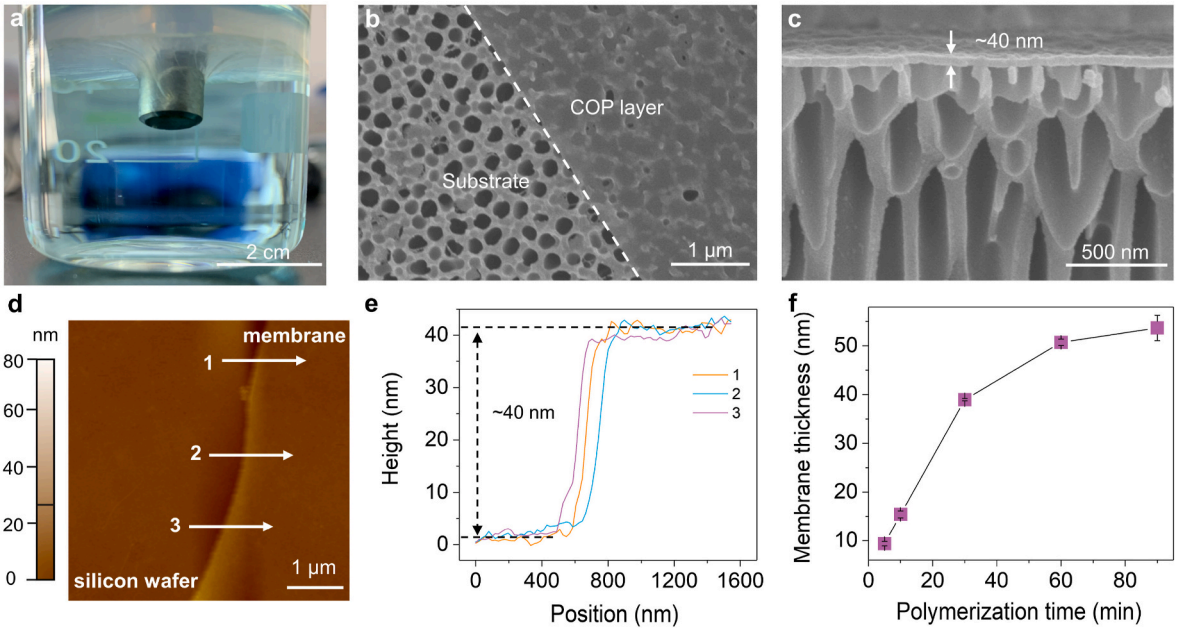

Fig. 2. Fabrication and characterization of free-standing COP membranes. (a) Photograph of the membrane formed at the interface with a duration of 10 min. (b) Surface SEM image of the membrane synthesized for 10 min. (c–e) Cross-sectional SEM image, AFM image, and the corresponding height profiles of the membrane synthesized for 30 min. (f) Membrane thickness as a function of synthesis duration. The height profiles in (e) correspond to the white lines in (d).

interface realizes the preparation and regulation of COP membranes.

Although support-free membranes can be produced at the interface, the poor mechanical robustness hinders their practical use in liquid separations. Thus, following the synthesis of membranes at the free interface, we sought to directly prepare COP selective layers on the top of porous substrates to generate composite membranes for robust separation. Thanks to their low cost, easy preparation, and flexibility, porous PAN substrates were selected as the substrates for synthesizing COP composite membranes. As schematically illustrated in Fig. 3a, after saturating the PAN substrate in the $Cu(NO_3)_2$ aqueous solution, the organic solution comprising of the monomer pairs is poured on the saturated substrate to perform rapid polymerization at room temperature. Such synthesis generates a shiny coverage with a diameter of ~4 cm on the PAN substrate (Fig. S6), indicating the formation of COP layers. As shown in Fig. 3b and c, the porous surface of PAN substrate can be completely covered by the grown COP membrane, thus forming a gate layer for selective separations. Moreover, extending the synthesis duration and increasing the concentration of catalyst in water both benefit for growing compact and dense composite membranes (Fig. S7). It is noted that the large particles on the surface of the membranes with

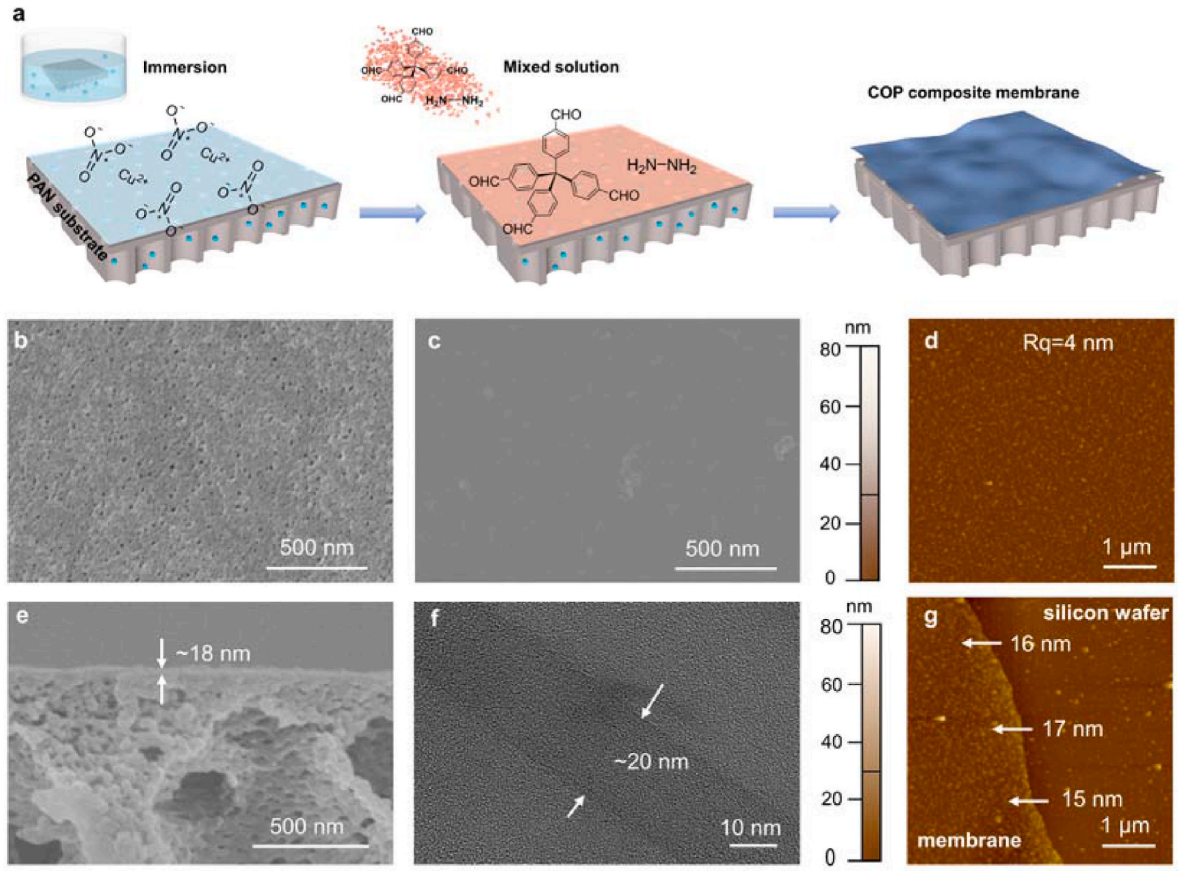

Fig. 3. Preparation and characterization of COP composite membranes. (a) Schematic illustration for the preparation of composite membranes. (b) Surface SEM image of the PAN substrate. (c–f) Surface SEM, AFM, cross-sectional SEM, and TEM images of the COP composite membrane. (g) AFM image of the COP layers detached from the composite membrane. The membrane in (c–g) is synthesized at a $Cu(NO_3)_2$ concentration of 0.05 mol L^{-1} for 30 min.

the improved growth conditions can be attributed to the deposition of products generated in the bulk solution. As confirmed by the AFM analysis (Fig. 3d), the resultant membrane synthesized at 0.05 mol L^{-1} of $Cu(NO_3)_2$ for 30 min exhibits a smooth surface with a low surface roughness of ~4 nm. From the cross-sectional SEM image, we can observe a thin and continuous layer located on the PAN substrate (Fig. 3e). The TEM image further identifies a precise thickness of ~20 nm for the synthetic COP layer (Fig. 3f). The AFM determination of the PAN-degraded membrane shows a low thickness similar to that of the above results (Fig. 3g, Fig. S8), suggesting the uniformity of COP layers. We attribute this low thickness of COP layers to the synergy of Cu $(NO_3)_2$-catalyzed rapid polymerization and interface-enabled self-inhibited growth [50]. In addition, the $Cu(NO_3)_2$-catalyzed interfacial synthesis exhibits a favorable generality to produce various imine-linked COP membranes (Fig. S9).

Next, the structural composition and surface properties of the prepared COP composite membranes were probed by different characterization techniques. The FTIR spectra shown in Fig. 4a verify the characteristic stretching vibration of C═N at 1624 cm^{-1}, implying the successful fabrication of COP layers. Moreover, the inherent charge of the continuous COPs dominates the surface charge of composite membranes [51,52], thus giving a weak negatively charged surface due to the electronegative carbonyl oxygen from the unreacted aldehyde groups of TFPM (Fig. 4b). As for the surface wettability, the COP composite membrane gives a relatively hydrophobic surface compared to that of the PAN substrate (Fig. 4c), which is related to the abundant benzene rings in the framework of COPs. Interestingly, an extremely high affinity between our membrane and EtOH can be observed, which displays an EtOH contact angle as low as 18°. More importantly, EtOH can be rapidly absorbed by the resulting membrane (Fig. 4d), illustrating hydrophobic nanochannels for fast transport of organic solvents [53].

To optimize the performance of COP composite membranes, we carried out the synthesis of membranes under different conditions and assessed their performances accordingly. Here, the membrane performances were quantified by permeance of EtOH and rejection of AF (molecular weight = 585.5 g mol^{-1}) through a dead-end filtration cell. The results shown in Fig. 5a reveal that AF rejection rates above 93% can be achieved by all the resulting membranes. Such a high molecular selectivity can be ascribed to the fact that compact and defect-free membranes can be formed rapidly. The relatively clean membrane surface and UV–vis spectra reveal an insignificant contribution of adsorption to separations (Fig. S10). Interestingly, the pure EtOH permeance of membranes shows an evident dependence on the catalyst concentration and synthetic duration. To be specific, noticeable decreases of EtOH permeance can be observed when extending the synthesis duration from 10 to 50 min or rising the catalyst concentration from 0.05 to 0.2 mol L^{-1}. The observed tendency agrees well with the increase of membrane thicknesses. As imaged by AFM, the extended synthesis duration and increased catalyst concentration both lead to a correlated increase in the thickness of COP selective layers (Figs. S11a–f). More importantly, the EtOH permeance exhibits an approximately linear dependence on the reciprocal of membrane thicknesses (Figs. S11g and h). Thus, these thicker membranes produce lower EtOH permeances because the mass transport is strongly hampered by the extended transferring length [54].

The membrane synthesized at a $Cu(NO_3)_2$ concentration of 0.05 mol L^{-1} for 30 min, showing a high EtOH permeance of 14.5 L m^{-2} h^{-1} bar^{-1} and an excellent AF rejection of 99%, was then investigated particularly. As shown in Fig. 5b, the permeance of various solvents presents an inverse relationship with their viscosity, following the Hagen-Poiseuille

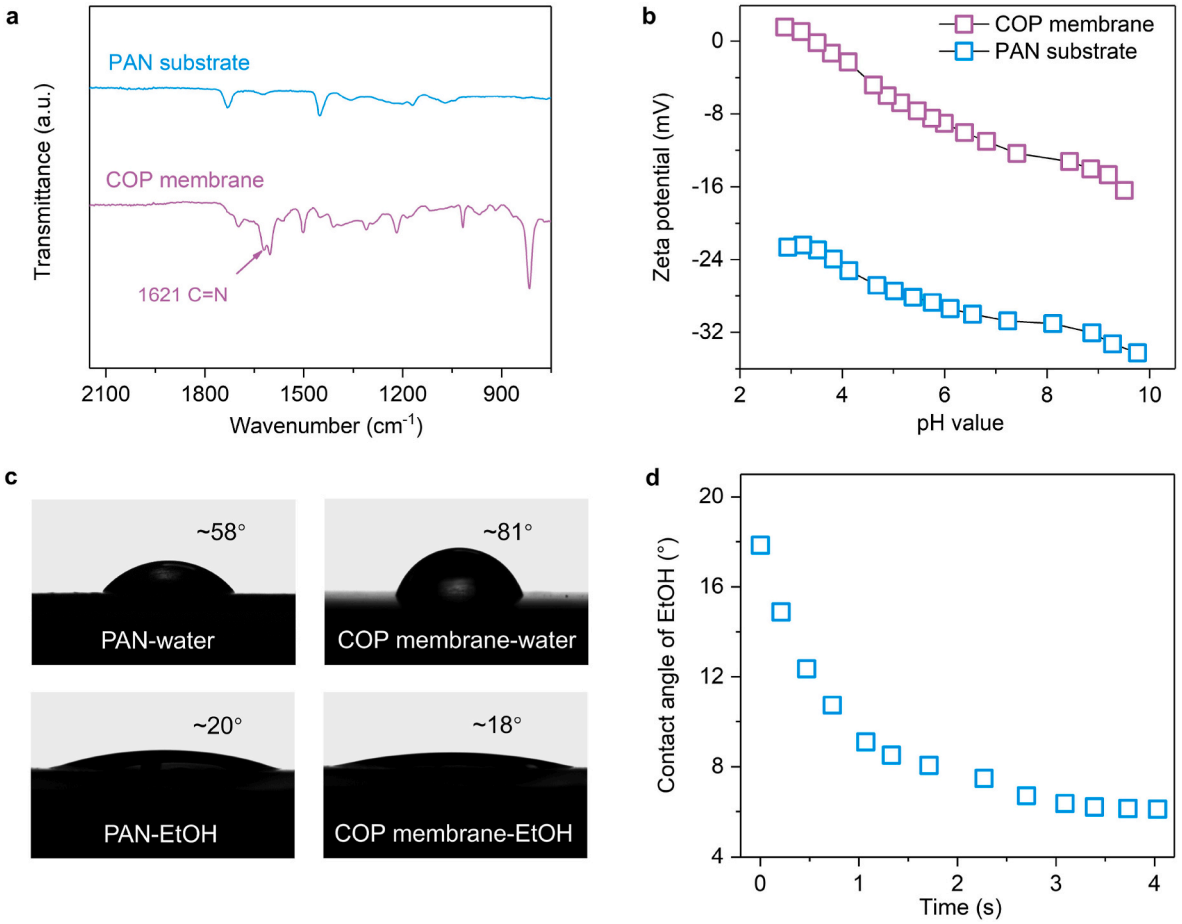

Fig. 4. Structural composition and surface property of the COP composite membrane. (a, b) FTIR spectra and Zeta potential curves of the PAN substrate and composite membrane. (c) Photographs of the water and EtOH contact angles. (d) Change of the EtOH contact angle with time for the COP composite membrane. The membrane in (a–d) is synthesized at a $Cu(NO_3)_2$ concentration of 0.05 mol L^{-1} for 30 min.

equation as the previously reported studies [55]. The permeance divergence for the solvents like hexane and acetonitrile could be related to the solvent polarity and interactions between solvents and membrane pore walls [56]. To profoundly explore the membrane selectivity, we carried out the filtration tests using a range of probe dyes with molecular weights ranging from ~287 to 961 g mol^{-1} (Fig. S12). Fig. 5c depicts the rejection profiles of small molecules in EtOH and MeOH. It is obvious that our membrane exhibits high rejection rates (>95%) to the solutes with a molecular weight above 500 g mol^{-1} (Figs. S13 and S14). The difference of rejections to the solutes with a molecular weight below 400 g mol^{-1} could be attributed to the diversity of electrostatic interactions in solvents (Fig. S15). The rejection profiles identify dye molecular weight cutoffs of 388 and 400 g mol^{-1} in EtOH and MeOH, respectively. The observed membrane selectivity keeps basically constant in water (Fig. S16). We should note that the selectivity is comparable to that of membranes built of well-crystallized counterparts [57–59]. Moreover, our membrane generates a superior performance compared with state-of-the-art membranes prepared by novel materials (Fig. S17, Table S1). Such a high molecular selectivity together with notable EtOH permeance mostly benefits from the subnanometer but three-dimensionally interconnected mass transport channels of COPs [60]. In addition, the synthesized membrane affords an excellent adaptability to transmembrane pressures. As can be seen from Fig. 5d, the permeation flux of EtOH during filtration rapidly responds to the incrementally altered transmembrane pressures, and the AF rejection rate keeps above 95%. We notice a slight decrease in EtOH permeance during separation, which can be attributed to the increase of mass transfer resistance with the presence of solutes. The separation performance remains largely stable with the transmembrane pressure of up to 10 bar (Fig. S18), comparable to the previously reported studies [61,62]. More importantly, the membrane pores constructed by covalently linked networks basically sustain their initial structure, thus allowing a long-term filtration for 150 h in the absence of significant deterioration (Fig. 5e, Fig. S19). These stability tests demonstrate the potential of our membrane in practical applications [63].

Encouraged by the convenience of membrane synthesis as well as decent membrane performances, we explored the feasibility of producing large-size COP membranes. As expected, we successfully scaled up the membrane size to 20 × 10 cm^2 using a home-made preparation module (Fig. 5f, Fig. S20). The large-size membrane offers a compact surface with no observation of pinholes or defects (Fig. S21). Moreover, the randomly selected membrane coupons exhibit similar EtOH permeance and AF rejection with that of the membranes discussed before (Fig. 5g). Thus, our strategy promises the production of large-size COP membranes and we expect the industrial manufacture of COP membranes through well-developed interfacial polymerization technology.

4. Conclusions

In summary, we have demonstrated the efficient catalysis of transition-metal nitrates ($Cu(NO_3)_2$) for rapidly synthesizing amorphous covalent organic polymers with uniform pores at room temperature. Through the condensation of tetrahedral aldehydes with linear amines, a highly microporous COP with three-dimensionally interconnected subnanometer channels is achieved. We reveal that the high-efficiency catalysis of $Cu(NO_3)_2$ is applicable for promptly polymerizing

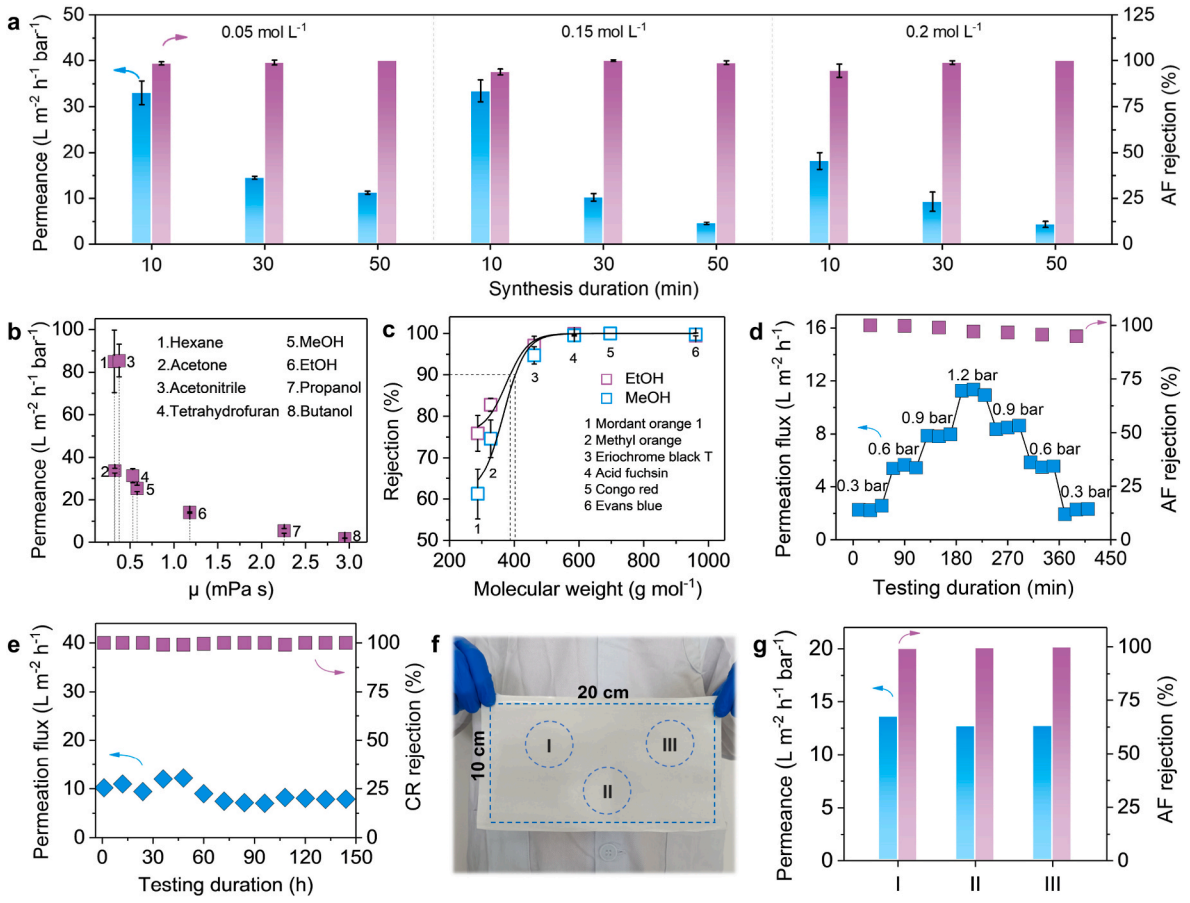

Fig. 5. OSN performances of COP composite membranes. (a) EtOH permeance and AF rejection of membranes versus catalyst concentration and synthesis duration. (b) Pure solvent permeance as a function of viscosity. (c) Rejection of dyes with different molecular weights in EtOH and MeOH. (d) Permeation flux and AF rejection in EtOH versus applied pressures. (e) OSN performance in long-term filtration. (f, g) Photograph and performance of the large-size COP composite membrane. The serial numbers in (g) correspond to the mark number in (f). The membrane in (b–g) is synthesized at a $Cu(NO_3)_2$ concentration of 0.05 mol L^{-1} for 30 min.

monomers at the organic-aqueous interface to generate COP membranes. More importantly, the designed interfacial method enables the direct preparation of COP separation membranes on porous substrates. The synthesized composite membranes exhibit an ultrathin layer of COPs and a relatively hydrophobic structure because of aromatic skeletons. With these unique benefits, the optimal COP composite membrane yields an excellent separation performance toward small molecules together with fast permeation of EtOH. The covalently linked frameworks permit stable operation of membranes under various transmembrane pressures and long durations without significant change of performances. This highly efficient synthesis strategy eventually allows the production of large-size COP composite membranes with an area of 200 cm^2 with no sacrifice of separation performance. This work thus offers a viable method for efficiently producing COP membranes and highlights the significance of amorphous but porous polymers in building potent liquid separation membranes.

Author statement

Jianghai Long: Investigation, Data curation, Writing-original draft, Writing-review & editing, Validation.

Xiansong Shi: Supervision, Investigation, Data curation, Writing-original draft, Writing-review & editing.

Tong Ju: Investigation, Methodology.

Xingyuan Wang: Investigation, Validation.

Zhe Zhang: Methodology, Validation.

Yong Wang: Conceptualization, Supervision, Writing-review & editing, Funding Acquisition.

All authors have approved to the final version of the manuscript.

Declaration of competing interest

The authors declare that they have no known competing financial interests or personal relationships that could have appeared to influence the work reported in this paper.

Data availability

Data will be made available on request.

Acknowledgments

This work was financially supported by the National Key Research and Development Program of China (2022YFB3805201).

Appendix A. Supplementary data

Supplementary data to this article can be found online at https://doi.org/10.1016/j.memsci.2023.121880.

References

[1] S. Chisca, V.-E. Musteata, W. Zhang, S. Vasylevskyi, G. Falca, E. Abou-Hamad, A.-H. Emwas, M. Altunkaya, S.P. Nunes, Polytriazole membranes with ultrathin tunable selective layer for crude oil fractionation, Science 376 (2022) 1105–1110.

[2] D.J.C. Constable, C. Jimenez-Gonzalez, R.K. Henderson, Perspective on solvent use in the pharmaceutical industry, Org. Process Res. Dev. 11 (2007) 133–137.

[3] Y. Li, J.Y. Zhu, S. Li, Z. Guo, B.V.d. Bruggen, Flexible aliphatic-aromatic polyamide thin film composite membrane for highly efficient organic solvent nanofiltration, ACS Appl. Mater. Interfaces 12 (2020) 31962–31974.
[4] N.A. Stini, P.L. Gkizis, C.G. Kokotos, Cyrene: a bio-based novel and sustainable solvent for organic synthesis, Green Chem. 24 (2022) 6435–6449.
[5] J. Geens, B.D. Witte, B.V.d. Bruggen, Removal of API's (active pharmaceutical ingredients) from organic solvents by nanofiltration, Separ. Sci. Technol. 42 (2007) 2435–2449.
[6] L.Q. Zhang, J. Wang, Y. Zhang, J.Y. Zhu, J.H. Yang, J.T. Wang, Y.T. Zhang, Y. Wang, Leaf-veins-inspired nickel phosphate nanotubes-reduced graphene oxide composite membranes for ultrafast organic solvent nanofiltration, J. Membr. Sci. 649 (2022), 120401.
[7] R.P. Lively, D.S. Sholl, From water to organics in membrane separations, Nat. Mater. 16 (2017) 276–279.
[8] H.A.L. Phuong, C.F. Blanford, G. Szekely, Reporting the unreported: the reliability and comparability of the literature on organic solvent nanofiltration, Green Chem. 22 (2020) 3397–3409.
[9] P. Vandezande, L.E. Gevers, I.F. Vankelecom, Solvent resistant nanofiltration: separating on a molecular level, Chem. Soc. Rev. 37 (2008) 365–405.
[10] G.M. Shi, Y.G. Feng, B.F. Li, H.M. Tham, J.Y. Lai, T.S. Chung, Recent progress of organic solvent nanofiltration membranes, Prog. Polym. Sci. 123 (2021), 101470.
[11] D.S. Sholl, R.P. Lively, Seven chemical separations to change the world, Science 532 (2016) 435–437.
[12] Y.H. Jin, Q.Q. Song, N. Xie, W.G. Zheng, J. Wang, J.Y. Zhu, Y.T. Zhang, Amidoxime-functionalized polymer of intrinsic microporosity (AOPIM-1)-based thin film composite membranes with ultrahigh permeance for organic solvent nanofiltration, J. Membr. Sci. 632 (2021), 119375.
[13] Z.J. Santanu Karan, Andrew G. Livingston, Sub-10 nm polyamide nanofilms with ultrafast solvent transport for molecular separation, Science 348 (2015) 1347–1351.
[14] Y. Li, Z. Guo, Sha Li, B.V.d. Bruggen, Interfacially polymerized thin-film composite membranes for organic solvent nanofiltration, Adv. Mater. Interfac. 8 (2020), 2001671.
[15] S.Y. Zhang, L. Shen, H. Deng, Q.Z. Liu, X.D. You, J.Q. Yuan, Z.Y. Jiang, S. Zhang, Ultrathin membranes for separations: a new era driven by advanced nanotechnology, Adv. Mater. 34 (2022), 2108457.
[16] J.Q. Yuan, X.D. You, N.A. Khan, R. Li, R.N. Zhang, J.L. Shen, L. Cao, M.Y. Long, Y. N. Liu, Z.J. Xu, H. Wu, Z.Y. Jiang, Photo-tailored heterocrystalline covalent organic framework membranes for organics separation, Nat. Commun. 13 (2022) 3826.
[17] I. Soroko, M.P. Lopes, A. Livingston, The effect of membrane formation parameters on performance of polyimide membranes for organic solvent nanofiltration (OSN): part A. effect of polymer/solvent/non-solvent system choice, J. Membr. Sci. 381 (2011) 152–162.
[18] D.Y. Xing, S.Y. Chanc, T.S. Chung, The ionic liquid [EMIM]OAc as a solvent to fabricate stable polybenzimidazole membranes for organic solvent nanofiltration, Green Chem. 16 (2014) 1383–1392.
[19] M.F.J. Solomon, Y. Bhole, A.G. Livingston, High flux membranes for organic solvent nanofiltration (OSN)—interfacial polymerization with solvent activation, J. Membr. Sci. 423–424 (2012) 371–382.
[20] K. Hendrix, G. Koeckelberghs, I.F.J. Vankelecom, Study of phase inversion parameters for PEEK-based nanofiltration membranes, J. Membr. Sci. 452 (2014) 241–252.
[21] C. Wang, M.J. Park, D.H. Seo, E. Drioli, H. Matsuyama, H. Shon, Recent advances in nanomaterial-incorporated nanocomposite membranes for organic solvent nanofiltration, Sep. Purif. Technol. 268 (2021), 118657.
[22] S. Xu, Y. Wang, Novel thermally cross-linked polyimide membranes for ethanol dehydration via pervaporation, J. Membr. Sci. 496 (2015) 142–155.
[23] S. Xu, L.F. Liu, Y. Wang, Network cross-linking of polyimide membranes for pervaporation dehydration, Sep. Purif. Technol. 185 (2017) 215–226.
[24] X.X. Loh, M. Sairam, A. Bismarck, J.H.G. Steinke, A.G. Livingston, K. Li, Crosslinked integrally skinned asymmetric polyaniline membranes for use in organic solvents, J. Membr. Sci. 326 (2009) 635–642.
[25] K. Vanherck, G. Koeckelberghs, I.F.J. Vankelecom, Crosslinking polyimides for membrane applications: a review, Prog. Polym. Sci. 38 (2013) 874–896.
[26] N. Manoranjan, F. Zhang, Z.Y. Wang, Y.P. Dong, W.X. Fang, Y.T. Zhang, Y.Z. Zhu, J. Jin, A single-walled carbon nanotube/covalent organic framework nanocomposite ultrathin membrane with high organic solvent resistance for molecule separation, ACS Appl. Mater. Interfaces 12 (2020) 53096–53103.
[27] N.A. Khan, R.N. Zhang, X.Y. Wang, L. Cao, C.S. Azad, C.Y. Fan, J.Q. Yuan, M. Y. Long, H. Wu, M.A. Olson, Z.Y. Jiang, Assembling covalent organic framework membranes via phase switching for ultrafast molecular transport, Nat. Commun. 13 (2022) 3169.
[28] Y.D. Cheng, S.J. Datta, S. Zhou, O. Shekhah, M. Eddaoudi, Advances in metal-organic framework-based membranes, Chem. Soc. Rev. 51 (2022) 8300–8350.
[29] S.S. Yuan, X. Li, J.Y. Zhu, G. Zhang, P.V. Puyveldeb, B.V.d. Bruggen, Covalent organic frameworks for membrane separation, Chem. Soc. Rev. 48 (2019) 2665–2681.
[30] H.Z. Dou, M. Xu, B.Y. Wang, Zhen Zhang, G.B. Wen, Y. Zheng, D. Luo, L. Zhao, A. P. Yu, L.H. Zhang, Z.Y. Jiang, Z.W. Chen, Microporous framework membranes for precise molecule/ion separations, Chem. Soc. Rev. 50 (2021) 986–1029.
[31] H.J. Wang, Y.M. Zhai, Y. Li, Y. Cao, B.B. Shi, R.L. Li, Z.T. Zhu, HaifeiJiang, Z. Y. Guo, M.D. Wang, L. Chen, Y.W. Liu, K.G. Zhou, F.S. Pan, Z.Y. Jiang, Covalent organic framework membranes for efficient separation of monovalent cations, Nat. Commun. 13 (2022) 7123.
[32] X.S. Shi, Z. Zhang, S.Y. Fang, J.T. Wang, Y.T. Zhang, Y. Wang, Flexible and robust three-dimensional covalent organic framework membranes for precise separations under extreme conditions, Nano Lett. 21 (2021) 8355–8362.
[33] C. Zhang, B.H. Wu, M.Q. Ma, Z.K. Wang, Z.K. Xu, Ultrathin metal/covalent-organic framework membranes towards ultimate separation, Chem. Soc. Rev. 48 (2019) 3811–3841.
[34] H.J. Wang, M.D. Wang, X. Liang, J.Q. Yuan, H. Yang, S.Y. Wang, Y.X. Ren, H. Wu, Z.Y. Jiang, Organic molecular sieve membranes for chemical separations, Chem. Soc. Rev. 50 (2021) 5468–5516.
[35] W.X. Lin, P.C. Wu, R.F. Li, J.H. Li, Y.M. Cai, L.H. Yuan, W. Feng, Novel triazine-based cationic covalent organic polymers for highly efficient and selective removal of selenate from contaminated water, J. Hazard Mater. 436 (2022), 129127.
[36] Z.H. Xiang, D. Cao, L.M. Dai, Well-defined two dimensional covalent organic polymers: rational design, controlled syntheses, and potential applications, Polym. Chem. 6 (2015) 1896–1911.
[37] A.A. Tashvigh, N.E. Benes, Covalent organic polymers for aqueous and organic solvent nanofiltration, Sep. Purif. Technol. 298 (2022), 121589.
[38] Z.H. Xiang, Y.H. Xue, D.P. Cao, L. Huang, J.F. Chen, L.M. DaI, Highly efficient electrocatalysts for oxygen reduction based on 2D covalent organic polymers complexed with non-precious metals, Angew. Chem. Int. Ed. 53 (2014) 2433–2437.
[39] J. Zheng, M. Wahiduzzaman, D. Barpaga, B.A. Trump, O.Y. Gutiérrez, P. Thallapally, S. Ma, B.P. McGrail, G. Maurin, R.K. Motkuri, Porous covalent organic polymers for efficient fluorocarbon-based adsorption cooling, Angew. Chem. Int. Ed. 60 (2021) 18037–18043.
[40] P. Puthiaraj, Y.-R. Lee, S. Zhang, W.-S. Ahn, Triazine-based covalent organic polymers: design, synthesis and applications in heterogeneous catalysis, J. Mater. Chem. 4 (2016) 16288–16311.
[41] N.B. McKeown, P.M. Budd, Polymers of intrinsic microporosity (PIMs): organic materials for membrane separations, heterogeneous catalysis and hydrogen storage, Chem. Soc. Rev. 35 (2006) 675–683.
[42] F. Alduraiei, S. Kumar, J.T. Liu, S.P. Nunes, G. Szekely, Rapid fabrication of fluorinated covalent organic polymer membranes for organic solvent nanofiltration, J. Membr. Sci. 648 (2022), 120345.
[43] D.Y. Zhu, Z.Q. Zhang, L.B. Alemany, Y. Li, N. Nnorom, M. Barnes, S. Khalil, M. M. Rahman, P.M. Ajayan, R. Verduzco, Rapid, ambient temperature synthesis of Imine covalent organic frameworks catalyzed by transition-metal nitrates, Chem. Mater. 33 (2021) 3394–3400.
[44] Y.Q. Qu, Y. Zha, H.G. Jia, Y. Zang, Y. Liu, T. Gu, X.Y. Du, Metal ion-catalyzed Interfacial polymerization of functionalized covalent organic framework films for efficient separation, Eur. Polym. J. 188 (2023), 111939.
[45] S. Kandambeth, V. Venkatesh, D.B. Shinde, S. Kumari, A. Halder, S. Verma, R. Banerjee, Self-templated chemically stable hollow spherical covalent organic framework, Nat. Commun. 6 (2015) 6786.
[46] H.L. Nguyen, C. Gropp, N. Hanikel, A. Mockel, A. Lund, O.M. Yaghi, Hydrazine-hydrazide-linked covalent organic frameworks for water harvesting, ACS Cent. Sci. 8 (2022) 926–932.
[47] Y.W. Peng, W.K. Wong, Z.G. Hu, Y.D. Cheng, D.Q. Yuan, S.A. Khan, D. Zhao, Room temperature batch and continuous flow synthesis of water-stable covalent organic frameworks (COFs), Chem. Mater. 28 (2016) 5095–5101.
[48] W.G. Lu, D.Q. Yuan, D. Zhao, C.I. Schilling, O. Plietzsch, T. Muller, S. Bräse, J. Guenther, J. Blümel, R. Krishna, Z. Li, H.C. Zhou, Porous polymer networks synthesis, porosity, and applications in gas storage separation, Chem. Mater. 22 (2010) 5964–5972.
[49] J. He, L.Z. Yu, Z.Y. Li, S.D. Ba, F. Lan, Y. Wu, Catalyst regulated interfacial synthesis of self-standing covalent organic framework membranes at room temperature for molecular separation, J. Colloid Interface Sci. 629 (2022) 428–437.
[50] K. Dey, M. Pal, K.C. Rout, S.K. H, A. Das, R. Mukherjee, U.K. Kharul, R. Banerjee, Selective molecular separation by Interfacially crystallized covalent organic framework thin films, J. Am. Chem. Soc. 139 (2017) 13083–13091.
[51] Z.F. Gao, J.T. Liu, T.S. Chung, Rapid in-situ growth of covalent organic frameworks on hollow fiber substrates with Janus-like characteristics for efficient organic solvent nanofiltration, Sep. Purif. Technol. 294 (2022), 121166.
[52] O. Setiawan, Y. Huang, Z.G. Abdi, W.S. Hung, T.S. Chung, pH-tunable and pH-responsive polybenzimidazole (PBI) nanofiltration membranes for Li^{+}/Mg^{2+} separation, J. Membr. Sci. 668 (2023), 121269.
[53] S. Li, R.J. Dong, V.-E. Musteata, J. Kim, N.D. Rangnekar, J.R. Johnson, B. D. Marshall, S. Chisca, J. Xu, S. Hoy, B.A. McCool, S.P. Nunes, Z.W. Jiang, A. G. Livingston, Hydrophobic polyamide nanofilms provide rapid transport for crude oil separation, Science 377 (2022) 1555–1561.
[54] Z. Jiang, S. Karan, A.G. Livingston, Water transport through ultrathin polyamide nanofilms used for reverse osmosis, Adv. Mater. 30 (2018), 1705973.
[55] L. Nie, K. Goh, Y. Wang, J. Lee, Y.J. Huang, H.E. Karahan, K. Zhou, M.D. Guiver, T.-H. Bae, Realizing small-flake graphene oxide membranes for ultrafast size-dependent organic solvent nanofiltration, Sci. Adv. 6 (2020), eaaz9184.
[56] P.H.H. Duong, Y.K. Shin, V.A. Kuehl, J.O.H. Mohammad, M. Afroz, B. Parkinson, A. C.T.v. Duin, K.D. Li-Oakey, Molecular interactions and layer stacking dictate covalent organic framework effective pore size, ACS Appl. Mater. Interfaces 13 (2021) 42164–42175.
[57] D.B. Shinde, L. Cao, A.D.D. Wonanke, S.K. Xiang Li, X.W. Liu, M.N. Hedhili, A.-H. Emwas, M. Addicoat, K.-W. Huang, Z.P. Lai, Pore engineering of ultrathin covalent organic framework membranes for organic solvent nanofiltration and molecular sieving, Chem. Sci. 11 (2020) 5434–5440.

[58] T.F. Huang, T. Puspasari, S.P. Nunes, K.-V. Peinemann, Ultrathin 2D-layered cyclodextrin membranes for high-performance organic solvent nanofiltration, Adv. Funct. Mater. 30 (2020), 1906797.
[59] R. Shevate, D.L. Shaffer, Large-area 2D covalent organic framework membranes with tunable single-digit nanopores for predictable mass transport, ACS Nano 16 (2022) 2407–2418.
[60] X.S. Shi, Z.p. Zhang, C.C. Yin, X. Zhang, J.H. Long, Z. Zhang, Y. Wang, Design of three-dimensional covalent organic framework membranes for fast and robust organic solvent nanofiltration, Angew. Chem. Int. Ed. 61 (2022), e202207559.
[61] X.R. Shui, J.Q. Li, M.X. Zhang, C.J. Fang, L.P. Zhu, Tailoring ultrathin microporous polyamide films with rapid solvent transport by molecular layer-by-layer deposition, J. Membr. Sci. 628 (2021), 119249.
[62] T.D. Lu, L.L. Zhao, W.F. Yong, Q. Wang, L. Duan, S.P. Sun, Highly solvent-durable thin-film molecular sieve membranes with insoluble polyimide nanofibrous substrate, Chem. Eng. J. 409 (2021), 128206.
[63] G. Szekely, M.F. Jimenez-Solomon, P. Marchetti, J.F. Kim, A.G. Livingston, Sustainability assessment of organic solvent nanofiltration: from fabrication to application, Green Chem. 16 (2014) 4440–4473.